GEOPHYSICAL RESEARCH LETTERS, VOL. ???, XXXX, DOI:10.1029/,

Electron Holes and Heating in the Reconnection Dissipation Region

H. Che,[1], J. F. Drake, M. Swisdak and P. H. Yoon

Che, H., J. F. Drake, and M. Swisdak, IREAP, Department of Physics, University of Maryland, College Park, MD, USA

J. F. Drake, and P. H. Yoon, IPST, University of Maryland, College Park, USA

[1]Current Address: Center for Integrated Plasma Studies (CIPS), Department of Physics, University of Colorado, UCB 390, Boulder, CO, USA

Using particle-in-cell simulations and kinetic theory, we explore the current-driven turbulence and associated electron heating in the dissipation region during 3D magnetic reconnection with a guide field. At late time the turbulence is dominated by the Buneman and lower hybrid instabilities. Both produce electron holes that co-exist but have very different propagation speeds. The associated scattering of electrons by the holes enhances electron heating in the dissipation region.

1. Introduction

Magnetic reconnection is the driver of explosive events in nature, such as solar flares, substorms in the magnetosphere of the Earth and flares from magnetars and the accretion disks of black holes. Satellite observations in the Earth's magnetosphere indicate that magnetic reconnection drives turbulence. Electron holes, which are localized, positive-potential structures caused by plasma kinetic instabilities, have been linked to current sheets associated with magnetic reconnection in the magnetotail [*Farrell et al.*, 2002; *Cattell et al.*, 2005; *Andersson et al.*, 2009], the magnetopause[*Matsumoto et al.*, 2003], and the laboratory[*Fox et al.*, 2008]. Lower hybrid (LH) waves and other plasma waves appear in conjunction with electron holes in the magnetotail events. Electron holes can scatter electrons, causing heating and possibly anomalous resistivity to facilitate fast magnetic reconnection.

During magnetic reconnection, a parallel electric field generated around the x-line drives electron beams. Simulations with a guide field show that these intense beams can drive the Buneman instability, which forms bipolar structures in the parallel electric field [*Drake et al.*, 2003]. Later in time transverse electric fields develop. Following a suggestion that these transverse fields were current-driven lower hybrid waves (LHI) [*McMillan and Cairns*, 2006], Che et al. [*Che et al.*, 2009] showed that both the LH and electron-electron two-stream instabilities resonate with the high velocity electrons and therefore dominate the interactions with the highest velocity electrons in narrow current layers. Which instabilities develop during reconnection and how they interact remains unknown.

During magnetic reconnection we demonstrate that two distinct classes of electron holes with very different propagation speeds exist simultaneously. Slow moving holes are driven by the Buneman instability and at the same time and locations fast moving holes are driven by the LHI. Both take the form of nonlinear Bernstein-Greene-Kruskal (BGK) solutions [*Bernstein et al.*, 1957] since the measured bounce time of electrons in the holes is short compared with the hole lifetime. The trapping and scattering of electrons by holes of disparate phase speed enhances dissipation during reconnection.

2. Simulation

We carry out 3D magnetic reconnection simulations with a strong guide field similar to those carried out earlier [*Drake et al.*, 2003] but with a much larger simulation domain: $L_x = 4d_i$, $L_y = 2d_i$, and $L_z = 4d_i$, where $d_i = c/\omega_{pi}$ and ω_{pj} is the plasma frequency of a particle species j. The reconnecting magnetic field is $B_x/B_0 = \tanh[(y - L_y/4)/w_0] - \tanh[(y-3L_y/4)/w_0]-1$, where B_0 is the asymptotic amplitude of B_x outside of the current layer, and w_0 is the half-width of the initial current sheet. The guide field $B_z^2 = B^2 - B_x^2$ is chosen so that the total field B is constant. In our simulation, B is taken as $26^{1/2}B_0$. The initial temperature is $T_e = T_i = 0.04m_ic_A^2$, the ion to electron mass ratio is 100, the speed of light c is $20c_A$ with $c_A = B_0/(4\pi n_0 m_i)^{1/2}$, the Alfvén speed. The initial drift speed of $4c_A$ is just above the electron thermal speed $3c_A$ and marginally exceeds the threshold to trigger the Buneman instability.

Magnetic reconnection induces a parallel electric field around the x-line and drives an intense electron beam. At $\Omega_it = 3$ ($\Omega_i = eB_0/m_ic$), the electron beams have been accelerated to $10c_A$ and to $14c_A$ at $\Omega_it = 4$. We show the current sheet around the x-line in the $x-y$ plane at $\Omega_i t = 3.3$ in Fig. 1 (a). At the beginning of the magnetic reconnection simulation, the Buneman instability with wavevector along the magnetic field z direction is excited. In the cold plasma limit, the phase speed is $(m_e/(2m_i))^{1/3}|v_{dz}|/2 \sim 1c_A$ and the growth rate is $\gamma \sim \sqrt{3}\omega_{pe}(m_e/(2m_i))^{1/3}/2 \sim 29\Omega_i$ [*Galeev and Sagdeev*, 1984]. The Buneman instability saturates within a short time. Later in time two distinct spatial structures of the electric field are observed: localized bipolar structures dominate E_z and long oblique stripes dominate E_x. A surprise is that there are two types of bipolar structures. At $\Omega_i t = 3$ one has a velocity close to zero and the other moves with a velocity of $3c_A$. By $\Omega_i t = 4$ the velocity of the second increases to $7c_A$. In Fig. 1 (b, c) we show E_z and E_x in the midplane $x - z$ of the current sheet at $\Omega_i t = 3.3$. The structures move to the left in this figure, which is in the direction of the electron drift. The downward (upward) arrows point to fast (slow) moving electron holes. To see the two classes of holes more clearly, in Fig. 2 (a, b) we stack cuts of $E_x(z)$ and $E_z(z)$ at the x-line versus time. The dark and light bands mark the development of the bipolar structures seen in Fig. 1 (b, c). The slopes of these bands are the phase speeds of the waves. During the time interval $\Omega_i t = 0 - 2$, the phase speed of the waves increases, which was expected since the streaming velocity of the electrons increased as the reconnection driven current layer shown in Fig. 1 (a) developed. During the time interval $\Omega_i t = 2 - 4$ two distinct phase speeds, particularly in E_z, are evident. In Fig. 2 (b) the structures cross each other at the same value of z, which indicates that this result is not due to the spatial structure of the streaming velocity. In Fig. 3 we show E_z and the $z - v_z$ phase space around $(x, y) = (1.2d_i, 1.5d_i)$ at $\Omega_i t = 3$ to reveal the structure of the fast moving holes.

There are no slow holes in this region at this time. In (a) the most intense hole is marked by the arrow. In (b) the center of the $z - v_{ez}$ phase space of this bipolar structure is marked by the star. The electrons encircling the star indicate that electrons are trapped by the bipolar field. The strong electron heating due trapping is evident.

Electron holes in the simulation exhibit a complex dynmics: formation, dissipation and reformation. The lifetimes τ_l of the two classes of electron holes are distinct, around $0.1\Omega_i^{-1}$ and $0.2\Omega_i^{-1}$ for the fast and slow holes, respectively. In both τ_l exceeds the bounce time of the trapped electrons, $\tau_b \approx \sqrt{m_e\lambda_b}/\sqrt{2e\delta E_z} \sim 0.02\Omega_i^{-1}$, where λ_b is the characteristic wavelength of the electron hole. Thus, electron trapping takes place and we therefore interpret the holes as BGK structures. [*Bernstein et al.*, 1957].

3. Kinetic Model and Analytic Results

We now investigate which instabilities drive the two distinct types of holes by examining in more detail the development of streaming instabilities. Using two drifting Maxwellians to model the electron distribution and a single Maxwellian to model the ion distribution, we fit the distribution functions obtained from the simulations and substitute the theoretical fittings into the local dispersion function derived from kinetic theory for waves with $\Omega_i \ll \omega \ll \Omega_e$ [*Che*, 2009]:

$$1 + \frac{2\omega_{pi}^2}{k^2 v_{ti}^2}[1 + \zeta_i Z(\zeta_i)] + \frac{2(1-\delta)\omega_{pe}^2}{k^2 v_{te1}^2}[1 + I_0(\lambda)e^{-\lambda}\zeta_{e1}Z(\zeta_{e1})] + \frac{2\delta\omega_{pe}^2}{k^2 v_{te2}^2}[1 + I_0(\lambda)e^{-\lambda}\zeta_{e2}Z(\zeta_{e2})] = 0, \tag{1}$$

where $\zeta_i = (\omega - k_z v_{di})/kv_{ti}$, $\zeta_{e1} = (\omega - k_z v_{de1})/k_z v_{zte1}$, $\zeta_{e2} = (\omega - k_z v_{de2})/k_z v_{zte2}$, $\lambda = k_x^2 v_{xte}^2/2\Omega_e^2$, δ is the weight of the low velocity drifting Maxwellian, Z is the plasma dispersion function and I_0 is the modified Bessel function of the first kind with order zero.

The thermal velocity of species j is defined by $v_{tj}^2 = 2T_{tj}/m_j$ and drift speed by v_{dj}, which is parallel to the magnetic field (z direction). The electron temperature takes a different value along and across the magnetic field while the ions are taken to be isotropic.

The fitting parameters of the distribution functions at $\Omega_i t = 3, 4$ are listed in Table 1. The match between the parallel distribution and our fitted distribution is shown in Fig. 4 (a). We can see from the Table that the weight δ of the low velocity electrons increases with time, indicating that momentum is transferred from the high velocity to the low velocity electrons.

The theoretical 2D spectrum at $\Omega_i t = 3$ is shown in Fig. 4 (b). Two distinct modes are found, one with $\mathbf{k}$ parallel and the other with $\mathbf{k}$ nearly perpendicular to $\mathbf{B}$. The peak of the parallel mode is around $k_z d_i \sim 20$, which is close to the wavenumber of the cold plasma limit of the Buneman instability, $k_z d_i = \omega_{pe}/v_{de} \sim 20$. To confirm that the parallel mode is the Buneman instability rather than the two-stream instability, we exclude ions from our calculations. The mode obtained only with electrons is shown in Fig. 4 (c). The two-stream instability has a much smaller growth rate. Thus, the parallel mode is the Buneman instability. The peak of the nearly-perpendicular mode is centered at $(k_x d_i, k_z d_i) = (22, 5)$. The frequency of this mode is $\sim 13\Omega_i$ which is in the LH frequency range for the present simulation so the nearly-perpendicular mode is the LHI [*McMillan and Cairns*, 2006; *Che et al.*, 2009].

As a test of this interpretation, we compare the phase speed of the modeled waves across (v_{px}) and along (v_{pz}) $\mathbf{B}$ with the simulation data. The assumption here is that since the fraction of trapped electrons in any given electron hole is small, the non-trapped particles control the phase speeds of the wave and the linear dispersion characteristics can be used to interpret hole propagation. It is well known that the Buneman instability can form parallel bipolar structures. This instability, which has a very low parallel phase speed to enable coupling to the ions, is the source of the electron holes moving slowly parallel to the magnetic field. Thus, the LHI should be responsible for the oblique, fast-moving electron holes marked by the downward arrows in E_z and the oblique stripes in E_x in Fig. 1. This interpretation is consistent with the parallel phase speeds v_{pz} of the Buneman and LH instabilities obtained by the kinetic model which are shown in Fig. 2 (c). The phase speed of the Buneman instability with $\theta \sim 0$ is close to zero. The three arrows from left to right (black,red and green) indicate the position θ of the maximum-growing mode of the LH instability at $\Omega_i t = 1, 3, 4$ shown in Fig. 2. The phase speed of the LH instability is initially low and then increases to $4c_A$ at $\Omega_i t = 3$ and to $7c_A$ at $\Omega_i t = 4$. The high phase speed of the LHI is consistent with the fast-moving electron holes seen at late time in the simulation. As a further check on this interpretation, in Fig. 5 (a) we stack the cuts of $E_x(x)$ along x at different times. The slope of the curves is the phase speed v_{px}. We see that at $\Omega_i t = 3$ $v_{px} \sim 0.6c_A$. In (b) is the theoretical phase speed v_{px} at $\Omega_i t = 1, 3, 4$ calculated from the model. At $\Omega_i t = 3$ the v_{px} of the LH wave, marked with the "*", is around $0.6c_A$, consistent with the value from the simulation.

4. Conclusion

In summary, we have demonstrated through simulations and an analytic model that two distinct classes of electron holes are generated simultaneously in the intense current layers that form during magnetic reconnection. The sources of the holes are the Buneman and

LHI. The LH waves produce a transverse field E_x as well as the bipolar structures E_z that trap electrons to form electron holes. These electron holes move along the magnetic field at the phase speed of the LH wave. Electron holes formed by the Buneman instability move more slowly. The simultaneous existence of electron holes with two distinct phase speeds enables electron scattering over a much larger range of velocity space than would be possible by either either instability alone. Electron dissipation in the intense current layers that form during reconnection is therefore enhanced. The LH electron hole was also independently observed by 2D Vlasov simulations [*Newman and Goldman*, 2008].

Acknowledgments. This work was supported in part by NSF ATM0613782, and NASA NNX08AV87G and NWG06GH23G. PHY acknowledges NSF grant ATM0837878. HC thanks Drs. M. Goldman and D. Newman for their helpful comments. The simulations were carried out at the National Energy Research Scientific Computing Center.

References

Andersson, L., et al. (2009), New Features of Electron Phase Space Holes Observed by the THEMIS Mission, Phys. Rev. Lett., *102*(22), 225,004–+, doi: 10.1103/PhysRevLett.102.225004.

Bernstein, I. B., J. M. Greene, and M. D. Kruskal (1957), Exact Nonlinear Plasma Oscillations, Physical Review , *108*, 546–550, doi:10.1103/PhysRev.108.546.

Cattell, C., et al. (2005), Cluster observations of electron holes in association with magnetotail reconnection and comparison to simulations, J. Geophys. Res., *110*, 1211–+, doi:10.1029/2004JA010519.

Che, H. (2009), Non-linear Development of Streaming Instabilities in Magnetic Reconnection with a Strong Guide Field, Ph.D. thesis, University of Maryland, College Park, United States – Maryland.

Che, H., J. F. Drake, M. Swisdak, and P. H. Yoon (2009), Nonlinear Development of Streaming Instabilities in Strongly Magnetized Plasma, Phys. Rev. Lett., *102*(14), 145,004–+, doi:10.1103/PhysRevLett.102.145004.

Drake, J. F., M. Swisdak, C. Cattell, M. A. Shay, B. N. Rogers, and A. Zeiler (2003), Formation of Electron Holes and Particle Energization During Magnetic Reconnection, Science, *299*, 873–877, doi:10.1126/*Science*.1080333.

Farrell, W. M., M. D. Desch, M. L. Kaiser, and K. Goetz (2002), The dominance of electron plasma waves near a reconnection X-line region, Geophys. Res. Lett., *29*(19), 190,000–1.

Fox, W., M. Porkolab, J. Egedal, N. Katz, and A. Le (2008), Laboratory Observation of Electron Phase-Space Holes during Magnetic Reconnection, Phys. Rev. Lett., *101*(25), 255,003–+, doi:10.1103/PhysRevLett.101.255003.

Galeev, A. A., and R. Z. Sagdeev (1984), Wave-particles interactions, in *Basic Plasma Physics: Selected Chapters, Handbook of Plasma Physics, Volume I*, edited by A. A. Galeev and R. N. Sudan, pp. 683–711.

Matsumoto, H., X. H. Deng, H. Kojima, and R. R. Anderson (2003), Observation of Electrostatic Solitary Waves associated with reconnection on the dayside magnetopause boundary, Geophys. Res. Lett., *30*(6), 060,000–1.

McMillan, B. F., and I. H. Cairns (2006), Lower hybrid turbulence driven by parallel currents and associated electron energization, Phys. Plasma, *13*(5), 052,104–+, doi: 10.1063/1.2198212.

Newman, D. L., and M. V. Goldman (2008), Perpendicular Localization of Electron Holes by Spatially Inhomogeneous Flows During Magnetic Reconnection*, *AGU Fall Meeting Abstracts*, pp. B1735+.

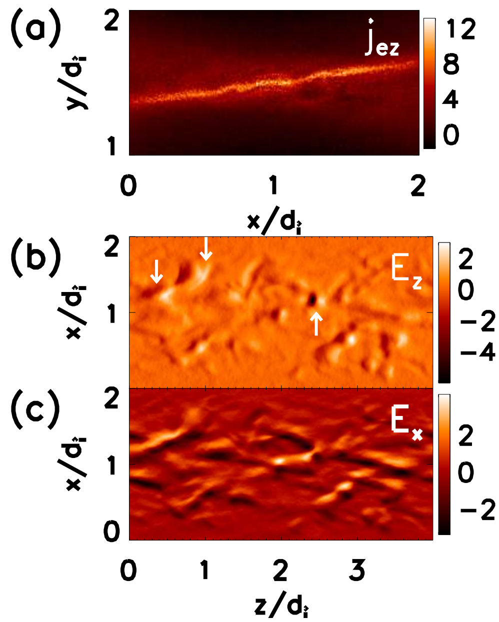

Figure 1. (**a**): The current sheet j_{ez} in the $x-y$ plane at $\Omega_i t = 3.3$. (**b, c**): The spatial structures of the electric fields E_x and E_z in the $x-z$ plane in a cut through the current layer.

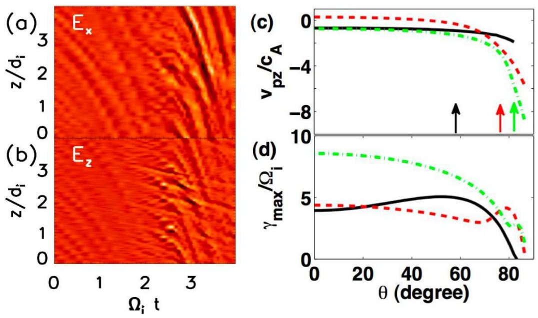

Figure 2. **(a, b)**: Cuts of $E_x(z)$ and $E_z(z)$ around the x-line at different times from the simulation. **(c)**: The theoretical parallel phase speed v_{pz} vs. the angle θ between wavevector **k** and magnetic field at $\Omega_i t = 1, 3, 4$ (black solid, red dashed and green dash-dotted lines). The arrows denote the angle θ of the fastest-growing mode of the LH instability at the three times in (d). **(d)** The theoretical growth rate γ_{max} of fast-growing mode vs. the angle θ at the three times in (c).

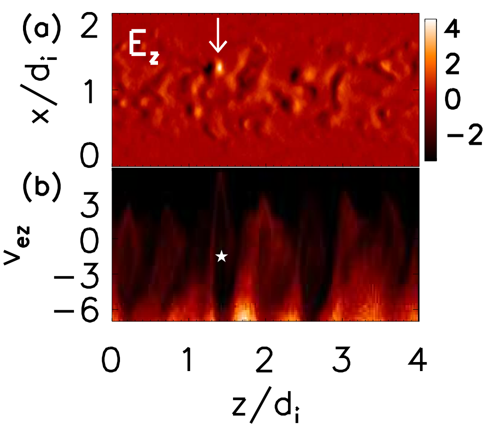

Figure 3. **(a)**: Spatial structure of E_z at $\Omega_i t = 3$ in the current layer. **(b)**: The phase space $z - v_{ez}$ at $x \sim 1.2$ of (a).

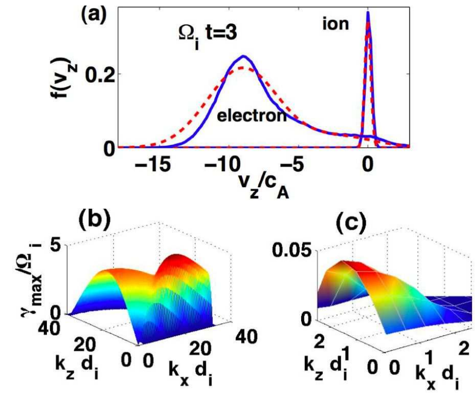

Figure 4. (**a**): Electron and ion distribution functions $f(v_z)$ around the x-line at $\Omega_i t = 3$ from simulations (blue solid) and the model (red-dashed) with the ion distribution function reduced by a factor of four. In (b) the 2D spectrum includes both electrons and ions and in (c) is without the ions.

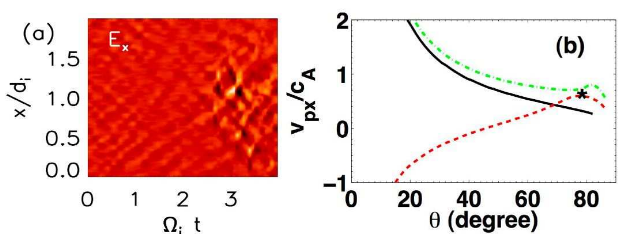

Figure 5. (**a**): Cuts of $E_x(x)$ at different times from the simulation. (**b**): Theoretical phase speed v_{px} vs. θ at $\Omega_i t = 1, 3, 4$, denoted by black solid, red-dashed and green dash-dotted lines.

Table 1. Parameters of Model Dist. Funs.

	v_{xte}	v_{zte1}	v_{zte2}	v_{de1}	v_{de2}	v_{ti}	v_{di}	δ
$\Omega_i t$= 3	2.8	3.6	3.5	-9.0	-2.0	0.3	0	0.16
$\Omega_i t$= 4	2.8	4.0	4.2	-9.0	-5.0	0.34	0.1	0.26